HEPATOBILIARY

Evaluation of perfusion CT and dual-energy CT for predicting microvascular invasion of hepatocellular carcinoma

Maïté Lewin[1,2] · Astrid Laurent-Bellue[2,3] · Christophe Desterke[2,4] · Adina Radu[1] · Joëlle Ann Feghali[1] · Jad Farah[1] · Hélène Agostini[5] · Jean-Charles Nault[6,7,8] · Eric Vibert[2,9,10] · Catherine Guettier[2,3,10]

Abstract

Purpose Evaluation of perfusion CT and dual-energy CT (DECT) quantitative parameters for predicting microvascular invasion (MVI) of hepatocellular carcinoma (HCC) prior to surgery.

Methods This prospective single-center study included fifty-six patients (44 men; median age 67; range 31–84) who provided written informed consent. Inclusion criteria were (1) treatment-naïve patients with a diagnosis of HCC, (2) an indication for hepatic resection, and (3) available arterial DECT phase and perfusion CT (GE revolution HD-GSI). Iodine concentrations (IC), arterial density (AD), and 9 quantitative perfusion parameters for HCC were correlated to pathological results. Radiological parameters based principal component analysis (PCA), corroborated by unsupervised heatmap classification, was meant to deliver a model for predicting MVI in HCC. Survival analysis was performed using univariable log-rank test and multivariable Cox model, both censored at time of relapse.

Results 58 HCC lesions were analyzed (median size 42.3 mm; range of 20–140). PCA showed that the radiological model was predictive of tumor grade ($p = 0.01$), intratumoral MVI ($p = 0.004$), peritumoral MVI ($p = 0.04$), MTM (macrotrabecular-massive) subtype ($p = 0.02$), and capsular invasion ($p = 0.02$) in HCC. Heatmap classification of HCC showed tumor heterogeneity, stratified into three main clusters according to the risk of relapse. Survival analysis confirmed that permeability surface-area product (PS) was the only significant independent parameter, among all quantitative tumoral CT parameters, for predicting a risk of relapse (Cox p value $= 0.004$).

Conclusion A perfusion CT and DECT-based quantitative imaging profile can provide a diagnosis of histological MVI in HCC. PS is an independent parameter for relapse.

Clinical trials ClinicalTrials.gov: NCT03754192.

Keywords Perfusion · Carcinoma · Hepatocellular · Microvascular invasion · Relapse · Radiomics

✉ Maïté Lewin
  maite.lewin@aphp.fr

[1] Service de Radiologie, AP-HP-Université Paris Saclay Hôpital Paul Brousse, 12-14 avenue Paul Vaillant Couturier, 94800 Villejuif, France

[2] Faculté de Médecine, Université Paris Saclay, 94270 Le Kremlin-Bicêtre, France

[3] Service d'Anatomopathologie, AP-HP-Université Paris Saclay Hôpital Bicêtre, 94270 Le Kremlin-Bicêtre, France

[4] Service de Bio-informatique, INSERM UA9, Hôpital Paul Brousse, 94800 Villejuif, France

[5] Service d'Epidémiologie et de Santé Publique, AP-HP-Université Paris Saclay Hôpital Bicêtre, 94270 Le Kremlin-Bicêtre, France

[6] Service d'Hépatologie, AP-HP, Hôpitaux Universitaires Paris-Seine-Saint-Denis, Hôpital Avicenne, 93000 Bobigny, France

[7] Functional Genomics of Solid Tumors Laboratory, Centre de Recherche Des Cordeliers, Sorbonne Université, Inserm, USPC, Université Paris Descartes, Université Paris Diderot, Université Paris 13, 75006 Paris, France

[8] Université Paris 13, Unité de Formation et de Recherche Santé Médecine et Biologie Humaine, 93000 Bobigny, France

[9] AP-HP-Université Paris Saclay, Hôpital Paul Brousse, 94800 Villejuif, France

[10] Centre Hépato-Biliaire, INSERM U1193 Hôpital Paul Brousse, 94800 Villejuif, France

Abbreviations

DECT   Dual-energy CT
DLP   Dose Length Product
HCC   Hepatocellular carcinoma
MVI   Microvascular invasion
MTM   Macrotrabecular-massive
PCA   Principal component analysis
HaBF   Hepatic arterial Blood Flow
HAF   Hepatic arterial flow
BF   Blood flow
BV   Blood volume
MSI   Mean slope of increase
TTP   Time to peak
MTT   Mean Transit Time
PS   Permeability surface-area produce
WHO   World Health Organization

Introduction

Vascular invasion, along with tumor size and the number of nodules, is a well-known major risk factor of early relapse of hepatocellular carcinoma (HCC) after surgical treatment [1, 2]. Macrovascular invasion can be detected by visualizing a tumor in the vein, whereas microvascular invasion (MVI) can only be microscopically detected. Furthermore, "macrotrabecular-massive" (MTM), a histological subtype of HCC that has been identified by recent studies, statistically correlated with MVI, is an independent predictor of early and overall relapse [3–5]. The role of preoperative imaging in assessing vascular invasion is still limited except when hepatic venous or portal venous tumor thrombus can be diagnosed [6, 7]. Some interesting studies have shown that suspicious qualitative imaging features, such as non-smooth tumor margins, internal arteries, mosaic architecture, irregular arterial rim-like enhancement, peritumoral arterial phase enhancement, and peritumoral hepatobiliary phase hypointensity, could predict MVI in HCC [8–14]. In order to improve imaging diagnosis of aggressive HCCs, recent studies have used radiomic analyses based on supervised machine-learning, in spite of major remaining challenges such as optimize feature extraction in radiological images [15–18].

Another approach to the prediction of preoperative vascular invasion is the use of quantitative imaging techniques. The results of perfusion computed tomography (CT) and dual-energy CT (DECT) data have been shown to be highly promising in the noninvasive assessment of tumor characteristics [19, 20]. Indeed, quantitative CT perfusion parameters, which are used to quantify tumor vascularity and angiogenesis in patients with HCC, reflect tumor aggressiveness and thus, could also help determine the prognosis [19, 21]. Furthermore, DECT-based iodine maps have been considered to be a potential perfusion biomarker of HCC [22]. Iodine-specific maps can reveal the presence or absence of local iodine in tissues and in the first case allow for its quantification [22]. It has been suggested that tumor response to anti-angiogenic therapy in patients with HCC may be predicted through the quantification of tumor iodine uptake as a biomarker of tumor vascularity [23]. Recent studies have also shown correlations between iodine density and some perfusion parameters in patients with HCC [24–26]. Therefore, the combined analysis of perfusion CT and DECT parameters assessing HCC tumor vascularity, should provide quantitative data in addition to the qualitative visual interpretation.

The study aims to evaluate perfusion CT and DECT quantitative parameters for predicting MVI of HCC prior to surgery.

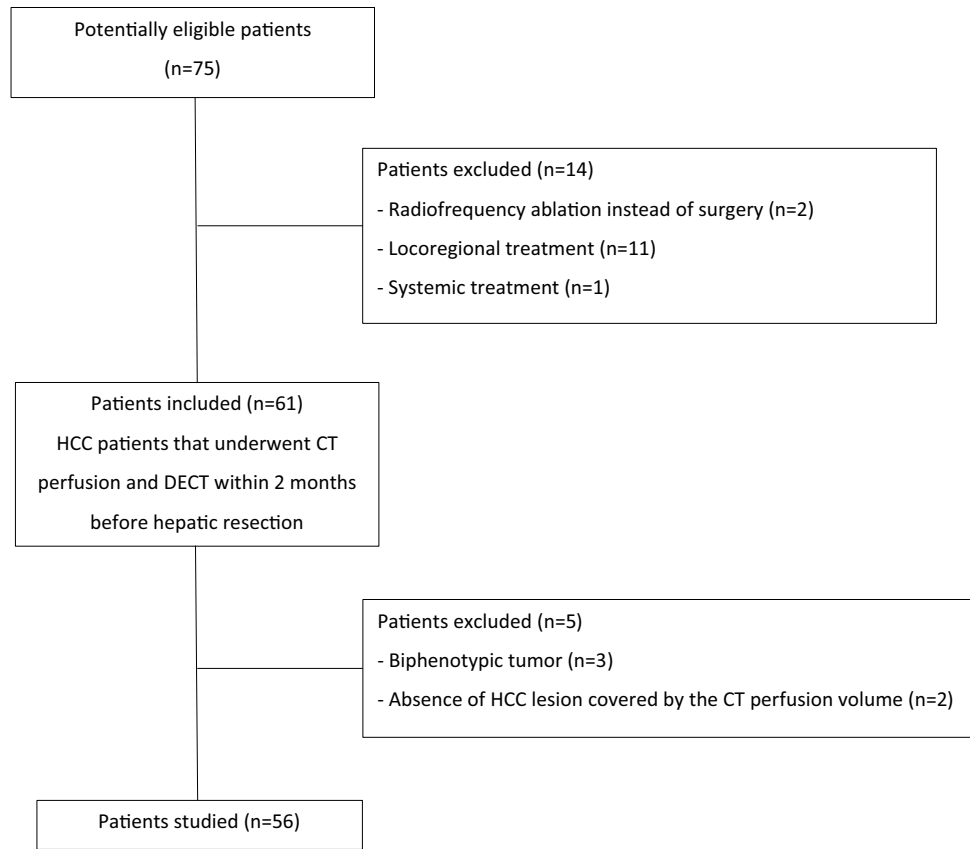## Materials and methods

Patients

Patients were prospectively and consecutively enrolled in this single-center study between December 2017 and March 2020, after providing written informed consent. The study was approved by the local institution review board. The study was registered with this provided number: ClinicalTrials.gov: NCT03754192. Inclusion criteria were (a) a diagnosis of HCC (≥ 20 mm) according to American Association for the Study of Liver Disease guidelines, (b) curative intent hepatic resection recommended by a multidisciplinary team, and (c) preoperative CT performed within 2 months prior to surgery in our radiology unit. Exclusion criteria were (a) previous locoregional or systemic HCC treatment, and (b) a contraindication to CT due to hypersensitivity to iodinated contrast media, renal failure estimated by a glomerular filtration rate < 30 ml/min or pregnancy.

According to literature data, the proportion of vascular invasion in a similar population has been estimated between 25 and 30%, which meant that 50 to 60 patients were required for the 15 MVI events needed to achieve univariate analysis of the radiological variables [27, 28].

Seventy-five patients were eligible but 14 patients were excluded because they received radiofrequency ablation instead of surgery ($n = 2$), locoregional ($n = 11$), or systemic ($n = 1$) HCC treatment. Five of the 61 remaining patients were excluded for the following reasons: biphenotypic tumor on histological analysis ($n = 3$) or failure to cover HCC lesion by the CT perfusion volume ($n = 2$) (Fig. 1). Thus, clinical data, alpha-fetoprotein (AFP) serum values and liver transient elastography results were obtained for the 56 included patients. All patients had a single solitary nodule, except for two patients with two nodules, which amounts to a total

Fig. 1 Flowchart of the study. *HCC* hepatocellular carcinoma, *DECT* dual-energy CT

Potentially eligible patients
(n=75)

Patients excluded (n=14)
- Radiofrequency ablation instead of surgery (n=2)
- Locoregional treatment (n=11)
- Systemic treatment (n=1)

Patients included (n=61)
HCC patients that underwent CT perfusion and DECT within 2 months before hepatic resection

Patients excluded (n=5)
- Biphenotypic tumor (n=3)
- Absence of HCC lesion covered by the CT perfusion volume (n=2)

Patients studied (n=56)

of 58 nodular-type HCC lesions. All patients were followed postoperatively to detect early tumor relapse within 3 years. For this, AFP serum levels were monitored and dynamic CT or MRI were performed every 6 months.

CT protocols

Patients underwent perfusion CT, followed by multiphase abdominal DECT with a 64-section multi-detector CT unit (Revolution HD GSI, GE Medical Systems Healthcare) ten minutes after the end of the perfusion image acquisitions. Unenhanced liver CT was first performed with a 140 mm-wide scan volume overlaying the HCC and the portal vein. Five seconds after administration of 45 ml of a non-ionic contrast agent (Iomeprol, 350 mg iodine /ml, Iomeron 350, Bracco Imaging) at a flow rate of 4 ml/sec followed by 20 ml of saline solution, perfusion CT was repeatedly performed in shuttle mode during normal breathing, with 25 volume acquisitions every 1.7 s over the first 42 s and then three volume acquisitions of 1.7 s every 30 s which amounts to a total examination time of 145 s (scan parameters: Table 1). Once perfusion acquisitions were complete, an arterial DECT phase (using bolus tracking software, acquisition began

Table 1 CT protocols

Parameters	No contrast	Perfusion CT	Arterial GSI	Portal phase	Delayed phase
Tube voltage (kV)	120	100	80–140	120	120
Tube current (mAs)	170–600	150	275–640*	170–600	170–600
Section collimation (mm)	40	40	40	40	40
Pitch factor	1.375	1.375	0.984	1.375	1.375
Reconstructed section thickness (mm)	1.25	5	1.25	1.25	1.25
Rotation time (s)	0.7	0.5	0.6	0.7	0.7
ASIR (%)	70	70	40	70	70

GSI Gemstone Spectral Imaging, *ASIR* Adaptive Statistical Iterative Reconstruction

*Fixed tube current adjusted to patient's BMI (body mass index)

6 s after the attenuation in abdominal aorta reached the threshold of 180 HU), a portal phase including a thoracic acquisition (60 s), and a delayed phase CT (3 min), were performed with administration of the same contrast agent (2 ml/kg minus the 45 ml already used for perfusion CT) at a flow rate of 4 ml/s (scan parameters: Table 1).

Perfusion CT and dual-energy CT data analysis

Results were processed at a workstation (Advantage Windows server 7.0, GE Medical Systems) by a radiologist (M.L with 15 years of experience in abdominal imaging) who was blinded to clinical and pathological data, using commercial CT perfusion software (GE CT perfusion 4D) for quantitative analyses. An integrated motion correction algorithm was first applied to all perfusion CT images and a deconvolution model with a dual vascular input algorithm was used to generate functional maps: Hepatic arterial Blood Flow (HaBF, in ml/100 g/min), Hepatic arterial flow (HAF, ratio between 0 and 1), Blood flow (BF, ml/100 g/min), Blood volume (BV, ml/100 g), Mean slope of increase (MSI, in HU/s), Tmax (seconds), Time to peak (TTP, seconds), Mean Transit Time (MTT, seconds), and Permeability surface-area product (PS,%). Iodine concentration maps were then automatically generated from arterial phase DECT images (GSI viewer, GE healthcare). The largest cross-sectional area of HCCs with the highest visual liver-to-lesion contrast were selected on perfusion CT images and regions of interest (ROI) were manually placed around the HCCs. Finally, all ROIs were automatically copied on parametric perfusion maps, iodine maps (arterial iodine concentration, IC (100 µg/ml)), and on arterial phase images (arterial density value, AD, (HU)) (Fig. 2). Similarly, standardized ROIs were drawn on the non-tumorous liver parenchyma and large hepatic vessels were avoided.

Patient exposure and radiation burden

Exposure parameters (DLP, mGy cm) were collected for perfusion, DECT, unenhanced, portal and delayed CT scan sequences using the Radiation Dose Monitor (RDM, Medsquare) Dose Archiving and Communication System (DACS).

Histopathologic analysis

Pathological examination of surgical specimens was simultaneously reviewed by two experienced liver pathologists (A.LB and C.G with 5 and 20 years' experience, respectively) and when interpretation was difficult a consensus was reached. Each nodule was analyzed for the following: (a) size, (b) presence of a capsule, (c) capsular invasion, (d) tumor differentiation according to a three-grade system (World Health Organization, WHO, 2019), (e) MVI defined as a tumor within a vascular space circled by endothelium, identified as intratumoral, peritumoral, or both, (f) satellite nodules, (g) the presence of an MTM component > 40%, (h) percent of tumor necrosis, (i) immunohistochemical expression of EpCAM (epithelial cell adhesion molecule) and AFP. In addition, the non-tumoral liver was assessed for steatosis (%) and fibrosis according to the METAVIR score.

Statistical analysis

Univariate logistic regression analyses were performed on tumor size and on each quantitative radiological perfusion parameter for testing MVI as outcome of the model. Concerning the radiological parameters, all data were integrated into two unsupervised multivariate models: principal component analysis (PCA) and unsupervised heatmap classification. First, PCA was performed with the FactoMineR R-package [29], only based on quantitative radiological parameters. Histological parameters were used as outcomes of the model. Significant Pearson correlations to
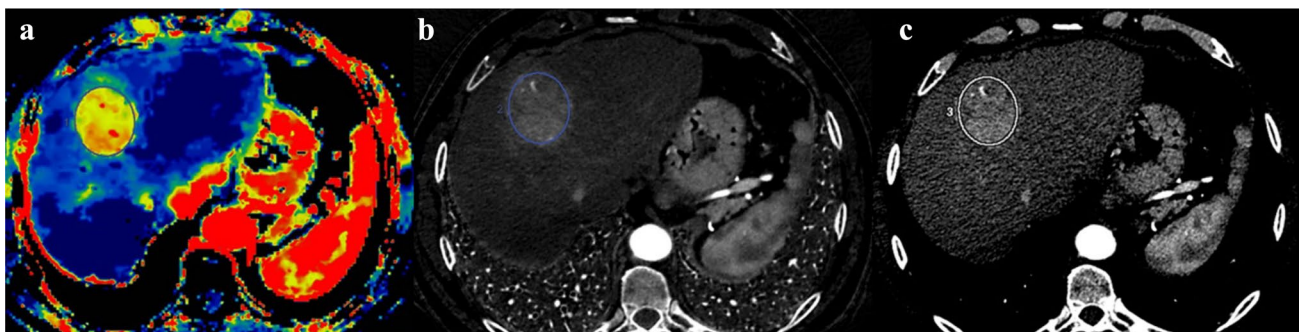

Fig. 2 Perfusion CT map (hepatic arterial blood flow) showing a manually placed region of interest (ROI) around the hepatocellular carcinoma (**a**). The ROI was automatically copied on to iodine maps (**b**) and arterial phase images (**c**)

pathological outcome parameters were extracted from PCA axes. In a second step, following the logarithm transformation of the radiological parameters, unsupervised classification was performed on a quantitative imaging heatmap using the ward_D2 method and Euclidean classification distances with illustrative integration of the histological parameters which were found to be significant using a PCA approach. The resulting unsupervised multivariate classification model was revealed as a heatmap using the pheatmap R-package [30]. When comparing mean values between different clusters for predictive radiological parameters, optimum binary cutoffs were selected for each significant parameter. Univariate survival analysis, censored at time of relapse, was performed using the log-rank test method for each stratification. Multivariable cox survival analysis, still censored at time of relapse, was performed with parameters that were identified as significant from univariate analysis (survival R-package). Statistical analysis was performed using a R-software (version 3.6.1) [31]. $p \leq 0.05$ was considered to be significant.

Results

Clinical and pathological characteristics of patients

Patient characteristics are summarized in Table 2. Most of the 56 patients were men (44/56, 78%), median age 67 years old (range 31–84) with chronic viral infection (21/56, 37.5%). All patients were classified according to the Barcelona-clinic liver cancer staging system as stage A. Two of the 56 patients had two tumors, which amounts to a total of 58 nodular-type HCC lesions [median size of 42.3 mm (range 20–140 mm)].

The pathological features of the tumors are summarized in Table 3. Most tumors were moderately differentiated (36/58, 62%). Intratumoral and peritumoral MVI were present in 20/58 (34%) and 25/58 (43%) of the tumors, respectively. The MTM component > 40% was observed in 11/58 (19%) of the tumors. A capsule was found in 46/58 (79%) and capsular invasion was present in 21/46 (45%) of these cases. The non-tumoral liver parenchyma was scored F3/F4 in 38/56 (68%) of the patients. The size of HCCs was significantly correlated to MVI ($p = 0.008$).

Tumor relapse occurred in 19/56 (34%) patients within a period of 6 month up to 3-year.

Perfusion CT and dual-energy CT quantitative analysis

Tumor and tumor-free liver parenchyma could be discriminated based on analysis of the eleven quantitative CT perfusion and DECT parameters (Table 4, Fig. 3). The AD, IC, HaBF, HAF, and MSI were significantly higher

Table 2 Patient characteristics

Variable	Value ($n = 56$ patients)
Age (years)	67 (31- 84)
Sex	
Male	44/56 (78%)
Female	12/56 (22%)
Weight (kg)	73 (45–106)
Height (cm)	171 (152–190)
Body mass index (kg/m^2)	24.9 (15.6–40)
Cirrhotic patients (Fibrosis F4)	20/56 (36%)
Risk factor for patients	
Chronic hepatitis B	9/56 (16%)
Chronic hepatitis C	12/56 (21%)
Alcohol abuse	9/56 (16%)
Metabolic syndrome	13/56 (23%)
Others	13/56 (23%)
HCC	
Number	58
Size (mm)	42.3 (20–140)
Alpha-fetoprotein (ng/ml)	6.95 (1–19,215)
Transient elastography (kPa)	7.1 (3.4–18)
Tumor relapse within 3 years	19/56 (34%)
Delay (years)	1 (0.6–3)

Data are presented as median values with ranges in parentheses or frequencies (%). HCC: hepatocellular carcinoma

in HCC lesions than in the tumor-free liver parenchyma while BV, Tmax, TTP, and MTT were significantly lower ($p < 0.001$). Univariate logistic regression performed on quantitative perfusion radiological parameters with MVI (intra and peritumoral MVI) did not reveal any significant association between the two. However, AD and the IC were significantly correlated to MVI (108 HU in HCC lesions with MVI versus 132 HU in HCC lesions without MVI, $p = 0.001$ and 27×100 µg/ml in HCC lesions with MVI versus 33×100 µg/ml in HCC lesions without MVI, $p = 0.015$, respectively) (Table 5).

The radiation burden from perfusion CT and GSI spectral imaging showed that the mean ± standard deviation DLP values for hepatic perfusion CT, arterial DECT, unenhanced, portal, and delayed CT scan sequences were 1309 ± 143, 462 ± 166, 286 ± 147, 666 ± 283, and 316 ± 160 mGy cm, respectively.

Prediction of histological parameters by the radiological model

The combination of the 11 quantitative parameters using PCA showed that a multivariate radiological model were predictive of the following histological features of

Table 3 Pathological features of hepatocellular carcinoma (HCC) nodules

Histopathological findings	$n = 58$ HCC
HCC nodules	
Major WHO grade	
Grade 3	4/58 (7%)
Grade 2	36/58 (62%)
Grade 1	18/58 (31%)
Intratumoral microvascular invasion	20/58 (34%)
Peritumoral microvascular invasion	25/58 (43%)
Macrotrabecular-massive subtype	11/58 (19%)
Capsular invasion	21/46 (45%)[a]
Necrosis > 30%	7/58 (12%)
Satellites nodules	21/58 (36%)
Immunochemistry EpCAM and AFP	10/58 (17%)–9/58 (15%)
Tumor free liver parenchyma for 56 patients	
Steatosis > 20%	11/56 (20%)
Fibrosis F0-1–2 versus F3-4	20/56 (36%) versus 38/56 (68%)

WHO World Health Organization

[a]Only 46/58 HCC had a tumor capsule

Table 4 Dual-energy CT (DECT) and Perfusion CT-derived quantitative parameters

CT parameters	HCC ($n = 58$)	Tumor free liver	p value
Arterial density (HU)	114.3 (63.1–225.6)	87.2 (32.8–138)	**< 0.001**
Iodine concentration (100 µg/ml)	29.47 (13.84–61.5)	14.27 (6.68–27.61)	**< 0.001**
Hepatic arterial blood flow (ml/100 g/min)	46.98 (13.37–188.7)	9.77 (0–271.1)	**< 0.001**
HAF (ratio between 0 and 1)	0.70 (0.15–0.99)	0.09 (0–0.81)	**< 0.001**
Blood flow (ml/100 g/min)	97.53 (40.95–507.9)	88.47 (31.75–260.5)	0.19
Blood volume (ml/100 g)	16.08 (5.18–43.62)	21.49 (6.79–35.62)	**< 0.001**
Mean slope of increase (HU/s)	1.69 (0.45–7.63)	0.67 (0.21–1.80)	**< 0.001**
T_{max} (s)	7.62 (3.781–13.16)	10.82 (2.68–22.15)	**< 0.001**
Time to peak (s)	23.29 (13.63–62.33)	36.11 (19.33–88.49)	**< 0.001**
Mean transit time (s)	12.14 (3.62–22.19)	18.82 (3.28–39.67)	**< 0.001**
Permeability surface-area product (%)	20.25 (0.073–104.8)	15.44 (0–123.1)	0.64

Data are presented as median values with ranges in parentheses

HCC hepatocellular carcinoma *HU* Hounsfield unit

Values in bold are significant

HCC: a major WHO grade ($p = 0.01$), intratumoral MVI ($p = 0.004$), peritumoral MVI ($p = 0.04$), a MTM component > 40% ($p = 0.02$), and capsular invasion ($p = 0.02$) (Fig. 4) with respective loadings on the first three dimensions: PCA1 (35.98%), PCA2 (23.10%), PCA3 (17.36%).

However, the radiological parameters were not found to be correlated to tumor necrosis, the presence of satellite nodules, immunohistochemical expression of EpCAM and AFP, or AFP serum values.

In addition, PCA showed that a non-tumoral multivariate radiological model could predict steatosis and fibrosis in the tumor-free liver parenchyma (steatosis > 20% and fibrosis F0-1-2 versus F3-F4 stratification scores, $p = 0.03$ and $p < 0.001$, respectively).

HCC classification using radiological model with selected pathological annotations

A heatmap classification of HCC nodules was obtained by the multivariate radiological model with selected pathological annotations (Fig. 5). Unsupervised classification showed that the association of these 11 quantitative parameters reflected tumor heterogeneity and that patients could be stratified into three main clusters (R1, R2, and R3). R1, the cluster on the left, showed a low recurrence
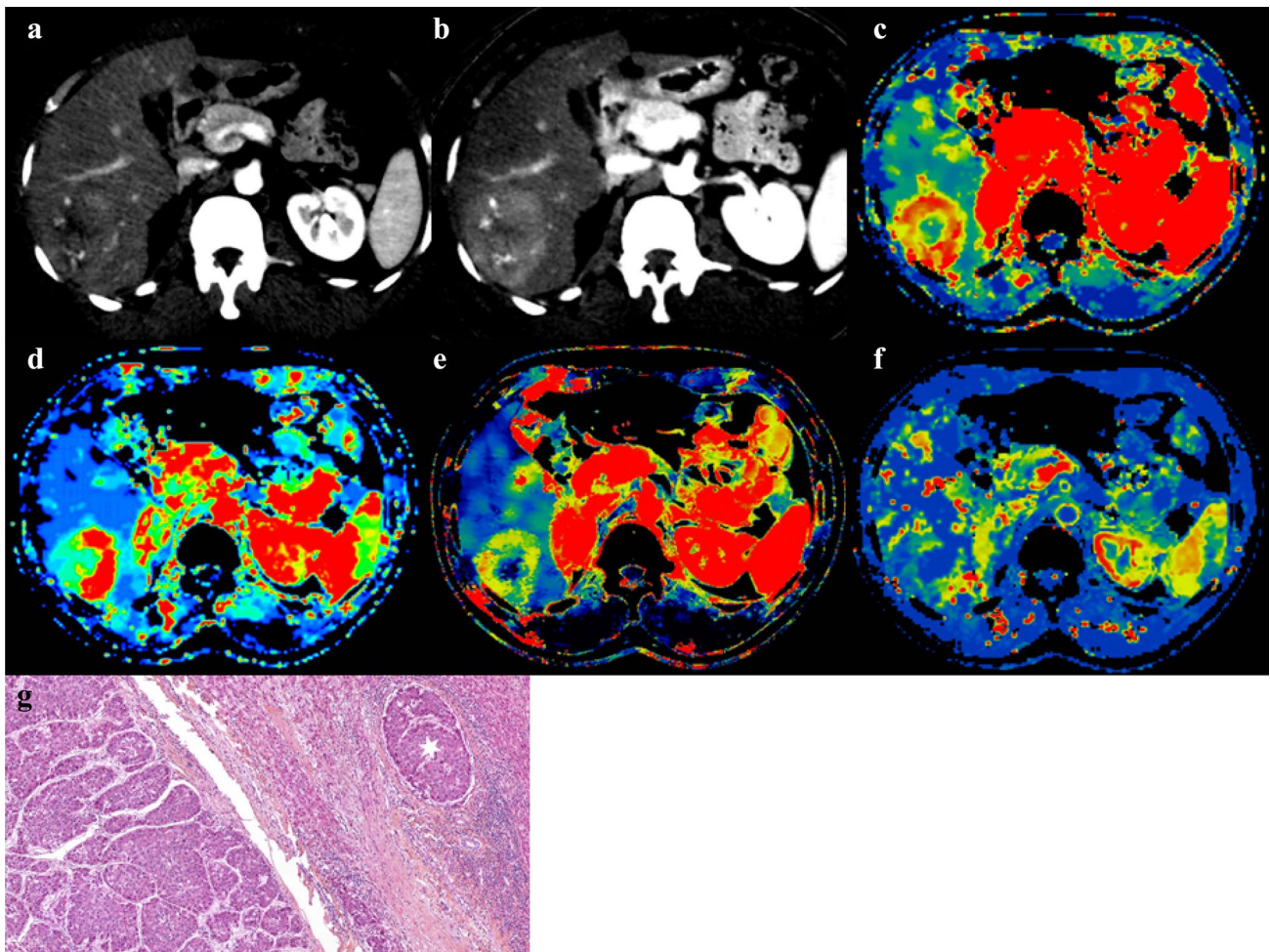
Fig. 3 Dual-energy CT (DECT) and Perfusion CT images in a 31-year-old man with hepatocellular carcinoma in hepatic segment VI. Axial images of **a** arterial phase, **b** iodine concentration, derived from multiphasic contrast-enhanced DECT. Axial parametric maps of **c** hepatic arterial blood flow (HaBF), **d** hepatic arterial flow (HAF), **e** mean slope of increase (MSI), and **f** permeability surface-area product (PS) obtained from perfusion CT. Liver resection specimen (hemato-eosin-saffron ×80). **g** the tumor shows a macrotrabecular liver architecture and microvascular invasion in peritumoral portal tract (star)

Table 5 Imaging parameters of HCC without microvascular invasion (MVI−) and HCC with microvascular invasion (MVI+)

CT parameters	MVI− (n = 28)	MVI+ (n = 30)	Total (n = 58)	p value
Arterial density (HU)	132.5 ± 35.7	108.4 ± 19	120 ± 30.6	**0.001194**
Iodine concentration (100 µg/ml)	32.7 ± 11.6	26.9 ± 5.8	29.7 ± 9.5	**0.015333**
Hepatic arterial Blood flow (ml/100 g/min)	61.9 ± 38.3	52.8 ± 24.9	57.2 ± 32.1	0.279120
HAF (ratio between 0 and 1)	0.7 ± 0.2	0.6 ± 0.3	0.6 ± 0.2	0.532659
Blood flow (ml/100 g/min)	127.3 ± 92.6	126.4 ± 89.4	126.8 ± 90.2	0.968128
Blood volume (mL/100 g)	18.7 ± 7.4	16.7 ± 7.3	17.7 ± 7.4	0.290894
Mean slope of increase (HU/s)	2.3 ± 1.4	1.8 ± 0.9	2.1 ± 1.2	0.104892
T_{max} (s)	7.8 ± 1.8	7.6 ± 2.1	7.7 ± 2	0.720924
Time to peak (s)	24.6 ± 9.5	26.8 ± 10.3	25.7 ± 9.9	0.413005
Mean transit time (s)	12.2 ± 4.5	12.2 ± 4.1	12.2 ± 4.3	0.954748
Permeability Surface-area product (%)	23 ± 25.9	30.8 ± 22.2	27.1 ± 24.1	0.215370

Data are presented as mean values ± standard deviations

HCC hepatocellular carcinoma, *HU* Hounsfield unit

MVI+ included intra-tumoral and peri-tumoral microvascular invasion

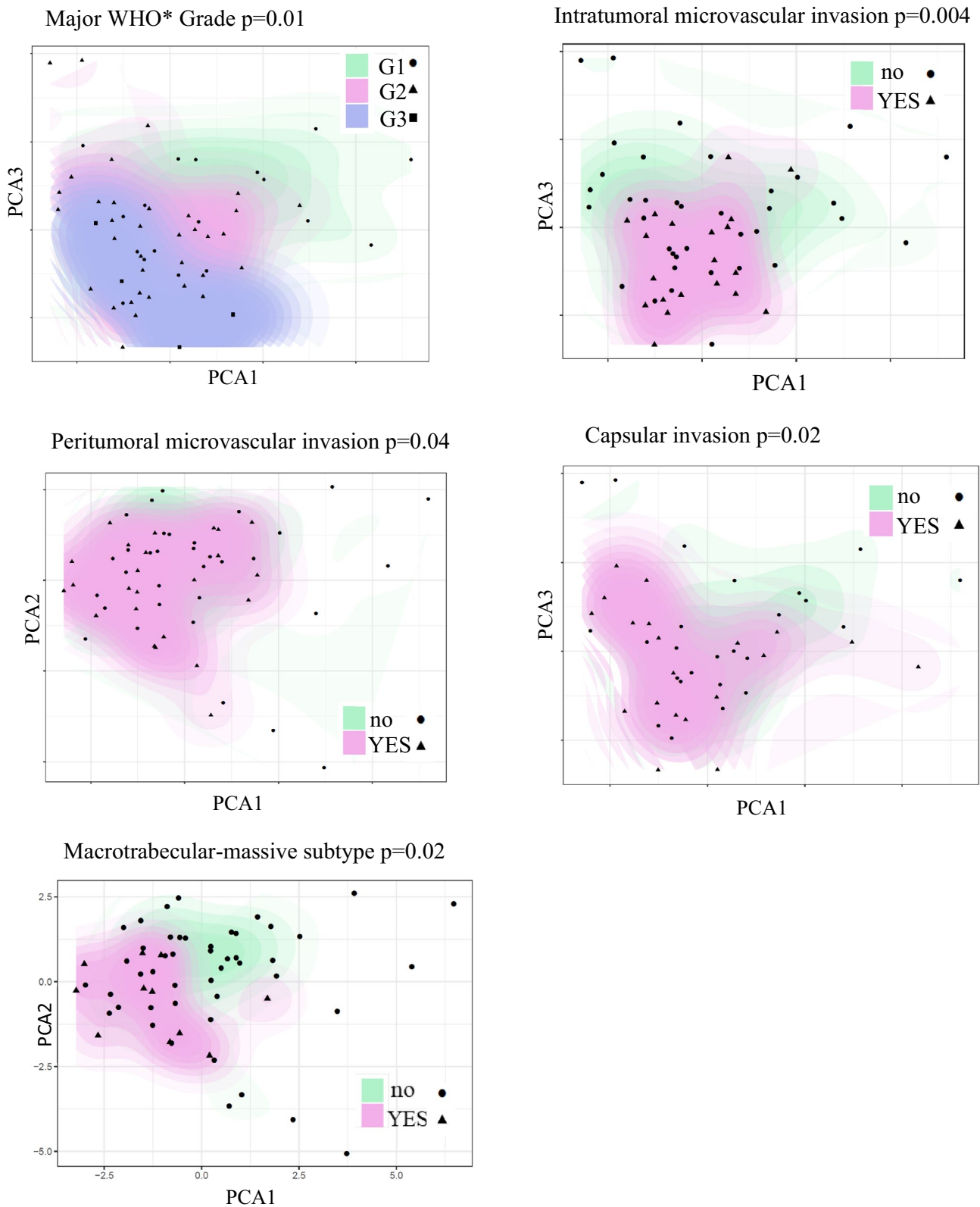Values in bold are significant

Fig. 4 Principal component analysis (PCA) projection of the multivariate radiological model with significant histological parameters. *WHO* World Health Organization
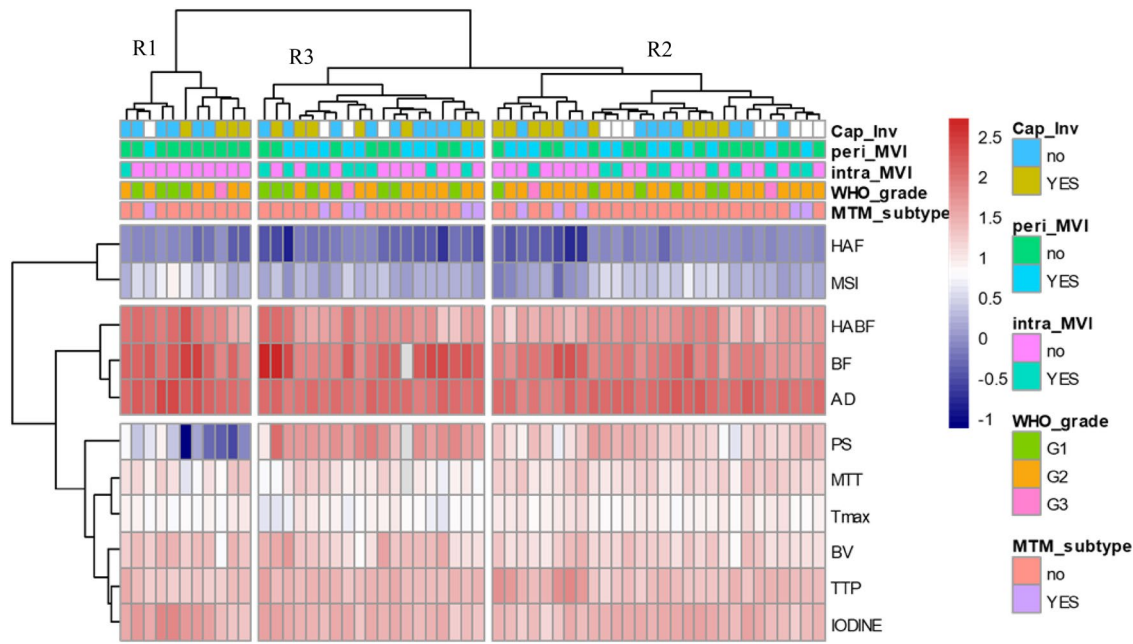
Fig. 5 Unsupervised classification on heatmap of 11 quantitative imaging parameters with pathological annotations: heatmap of cells representing radiological parameter quantifications with adjacent clustering performed by ward_D2 method and Euclidean distances. This clustering allowed patient stratification in three main clusters: R1on the left (characterized by a low level of PS), R2 on the right and R3 in the middle. *HAF hepatic arterial flow, MSI mean slope of increase, *HABF* hepatic arterial blood flow, *BF* blood flow, *AD* arterial density, *PS* permeability surface-area product, *MTT* mean transit time, *BV* blood volume, *TTP* time to peak, *peri_MVI* peritumoral microvascular invasion, *intra_MVI* intratumoral microvascular invasion, *Cap_Inv* capsular invasion, *WHO_grade* major World Health Organization grade, *MTM_subtype* macrotrabecular-massive subtype

risk due to the absence or a very rare occurrence of intra- and/or peritumoral MVI or MTM-subtype. The clusters R2 on the right and R3 in the middle which included most of the tumors, showed a higher risk of recurrence since most of them proved positive for intra- and/or peritumoral

MVI and a MTM component > 40%. Interestingly, the left-hand R1 cluster had a low level of PS. In contrast, the right-hand R2 cluster and the R3 middle cluster had medium and high levels of PS, respectively.

Table 6 Univariate and Multivariate analyses of radiological relapse risk factors

CT parameters	Threshold for worst prognostic	Univariate *p* values	Multivariate Cox *p*-values
Arterial density (HU)	< 120	0.009	0.16
Iodine concentration (100 μg/ml)	24.35	0.13	NA
Hepatic arterial Blood Flow (ml/100 g/min)	46.2	0.62	NA
HAF (ratio between 0 and 1)	0.8	0.52	NA
Blood flow (ml/100 g/min)	75	0.20	NA
Blood volume (mL/100 g)	20.5	0.80	NA
Mean slope of increase (HU/s)	1.53	0.21	NA
Tmax (s)	< 7.7	0.02	0.18
Time to peak (s)	> 23.2	0.01	0.05
Mean transit time (s)	10.3	0.471	NA
Permeability surface-area product (%)	> 22.79	< 0.001	**0.004**

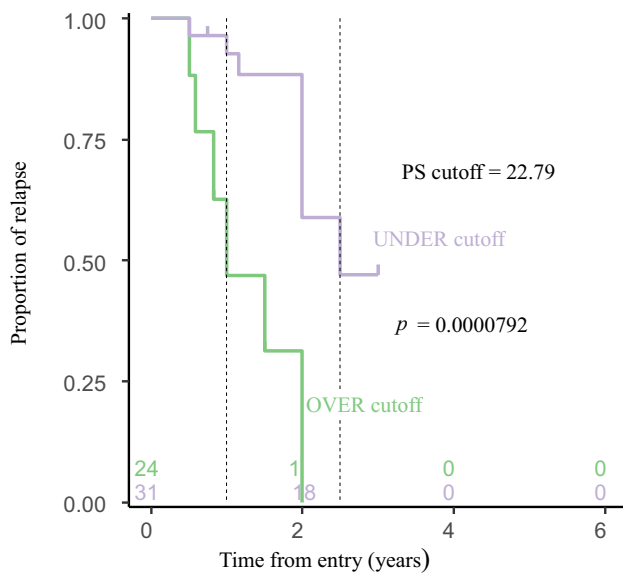NA: not applicable

Value in bold are significant

Fig. 6 Log-rank analysis on independent PS parameter censored at time of relapse

Association of early recurrence with quantitative radiologic parameters

Quantitative radiological parameters were ranked individually compared to relapse status (19/56, 34%) to evaluate their respective optimal threshold of stratification for survival analysis (Table 6). Four of the 11 quantitative radiological parameters were found to be significant on univariate analysis by the log-rank test. The thresholds for the parameters were 120 for AD (log-rank p value = 0.009), 22.79 for PS (log-rank p value < 0.001), 7.7 for Tmax (log-rank p value = 0.02), and 23.2 for TTP (log-rank p value = 0.01). To test the independence of these prognostic parameters, a Cox multivariate model was built including AD, PS, T_{max}, and TTP. In this model, only PS was found to be an independent and significant parameter to predict the risk of relapse (Cox p value = 0.004). According to the Log-rank analysis, if the PS value is > 22.79, the median estimated time to relapse is 1 year, otherwise the median time to relapse is > 2 years (Fig. 6).

Discussion

This study shows that an imaging profile using a combination of quantitative tumoral CT parameters obtained from perfusion CT and DECT can predict the presence of peritumoral and intratumoral MVI, capsular invasion, tumor grade, and the MTM-subtype in HCC. Moreover, this radiological profile can be used to determine tumor heterogeneity and identify different sub-groups of HCC associated with

specific histological features. PS appears to be the only independent prognostic parameter of the quantitative tumoral CT parameters that were tested.

By comparing our experimental quantitative CT perfusion and DECT results with the results in the literature, we obtained recognized values allowing us to build our radiologic model [21, 26, 32]. The imaging profile obtained with the 11 quantitative tumoral CT parameters was predictive of prognostic histological factors in HCC nodules. In fact, PCA identified a homogeneous, well-characterized group with significant invasive histological parameters (MVI, capsular invasion, MTM-subtype) that were also associated with WHO grade progression. Thus far, the only histological parameter identified using CT perfusion was reported by Sahani et al., who showed a significant difference in CT perfusion parameters between well-differentiated HCC and other grades ($p < 0.05$) [21]. Other approaches based on image descriptors have also been proposed for the prediction of MVI, such as radiogenomic venous invasion signatures on preoperative contrast-enhanced CT by Banerjee et al., or radiomic models based on texture analysis by Xu et al. and Ma et al., and a more recent model based on volumetric iodine quantification using DECT by Kim et al. [33–36]. But, to the best of our knowledge, there are no data on CT perfusion and MVI in HCC.

In our study intertumoral heterogeneity could be stratified with the quantitative imaging profile. Stratification helped identify patients at a high or low risk of relapse after hepatic resection, which could be used to determine specific therapeutic and management strategies in clinical practice. The performance of statistical models based on radiomic analysis has been shown to be good for the prediction of recurrence in early stage of HCC by Ji et al. [37]. The correlation between radiogenomics and the phenotype of aggressive disease and certain gene expression signatures on qualitative imaging has also been investigated by Taouli et al. [38]. However, none of these models are used in routine clinical practice. Conversely, the present study found that the preoperative tumor value of PS was an independent predictor of the risk of relapse. Interestingly, PS is a well-known parametric map reflecting tumor angiogenesis at varying degrees of maturation, which has mainly been used as a tumor response biomarker after targeted therapy, but not for preoperative prognosis [21, 39, 40]. It could be hypothesized that high PS values (> 22.79) suggest aggressive behavior in HCC due to the MVI or MTM-subtype.

The quantitative imaging profile could also be used to assess the non-tumoral liver and predict liver steatosis (threshold > 20%) and liver fibrosis (F0/F1/F2 fibrosis stages versus F3-4 stages). These same results were reported by Van Beers et al. in patients with cirrhosis [41]. In addition, Ronot et al., showed that perfusion CT can discriminate patients with early stages of liver fibrosis [42]. Incorporating

the noninvasive assessment of liver fibrosis and steatosis could help extend the selection criteria for HCC resection.

The patients in our study were exposed to higher radiations doses than with a standard dynamic study, which may be of concern. However, when the DLP values registered in our study are compared to national Diagnostic Reference Levels for chest-abdomen-pelvis CT ($DLP_{ref} = 750$ mGy cm) only perfusion CT acquisitions were found to exceed the limit, while arterial DECT were within reference levels. Nevertheless, we feel that these perfusion CT radiation doses can be justified and compensated by the benefits and added value of the diagnostic information. Indeed, PS preoperative data, provided by perfusion CT for identifying aggressive HCC may be beneficial for both therapeutic and prognostic purposes. This protocol must now be optimized in further studies by reducing the radiation dose while keeping a good quality image.

Our study definitively has some limitations. First, the number of patients was low and only surgically confirmed HCCs were included, which could create a selection bias. Secondly, a 64-section multi-detector was used, while a 256-detector row scanner might have improved the performance of perfusion analysis. Moreover, DLP values for arterial acquisition could be improved by adjusting tube current. Thirdly, there could be a potential element of confusion in DECT parameters (AD and IC), resulting from the residual contrast from previous injections of perfusion CT. Advanced fibrosis could also affect quantitative parameters of liver perfusion. Fourthly, 2D ROIs were used instead of volumes-of-interest, because we believe that the selected surface reflects the heterogeneity of HCC. Fifthly, even though a strong inter-reader agreement has already been reported on the basis of a standardized CT protocol with the same CT perfusion software, we have to admit that the inter-reader agreement was not evaluated in the measured quantitative parameters [24]. Finally, the reproducibility of this quantitative imaging profile was not evaluated in an external validation cohort, which means that further multicenter studies with other CT manufacturers are required, in order to validate this imaging profile before it can be used in routine clinical practice [43, 44].

In conclusion, this study presents an imaging profile using a combination of quantitative perfusion CT and DECT parameters to diagnose histological MVI and MTM-subtype in patients with HCC prior to surgery. The preoperative tumor value of PS is an independent predictor of patients at a high risk of relapse prior to treatment.

Declarations

References

1. Llovet JM, Kelley RK, Villanueva A et al (2021) Hepatocellular carcinoma. Nat Rev Dis Primers 7:6. https://doi.org/10.1038/s41572-020-00240-3

2. Imamura, H, Matsuyama Y, Tanaka E et al (2003) Risk factors contributing to early and late phase intrahepatic recurrence of hepatocellular carcinoma after hepatectomy. J Hepatol 38:200-7. https://doi.org/10.1016/s0168-8278(02)00360-4

3. Ziol M, Poté N, Amaddeo G et al (2018) Macrotrabecular-massive hepatocellular carcinoma: A distinctive histological subtype with clinical relevance. Hepatology 68:103-112. https://doi.org/10.1002/hep.29762

4. Calderaro J, Couchy G, Imbeaud S et al (2017) Histological subtypes of hepatocellular carcinoma are related to gene mutations and molecular tumour classification. J Hepatol 67:727-738. https://doi.org/10.1016/j.jhep.2017.05.014

5. Mulé S, Galletto Pregliasco A, Tenenhaus A et al (2020) Multiphase liver MRI for identifying the macrotrabecular-massive subtype of hepatocellular carcinoma. Radiology 295:562-571. https://doi.org/10.1148/radiol.2020192230

6. Choi JY, Lee JM, Sirlin CB (2014) CT and MR imaging diagnosis and staging of hepatocellular carcinoma : part I. Development, growth, and spread: key pathologic and imaging aspects. Radiology 272:635-54. https://doi.org/10.1148/radiol.14132361

7. Reginelli A, Vacca G, Segreto T et al (2018) Can microvascular invasion in hepatocellular carcinoma be predicted by diagnostic imaging? A critical review. Future Oncol 14:2985-2994. https://doi.org/10.2217/fon-2018-0175

8. Chou CT, Chen RC, Lin WC, Ko CJ, Chen CB, Chen YL (2014) Prediction of microvascular invasion of hepatocellular carcinoma: preoperative CT and histopathologic correlation. AJR Am J Roentgenol. 203:W253-9. https://doi.org/10.2214/AJR.13.10595

9. An C, Kim DW, Park YN, Chung YE, Rhee H, Kim MJ (2015) Single hepatocellular carcinoma: Preoperative MR imaging to predict early recurrence after curative resection. Radiology 276:433-43. https://doi.org/10.1148/radiol.15142394

10. Renzulli M, Brocchi S, Cucchetti A et al (2016) Can current pre-operative imaging be used to detect microvascular invasion of hepatocellular carcinoma? Radiology 279:432-42. https://doi.org/10.1148/radiol.2015150998

11. Lee S, Kim SH, Lee JE, Sinn DH, Park CK (2017) Preoperative gadoxetic acid–enhanced MRI for predicting microvascular invasion in patients with single hepatocellular carcinoma. J Hepatol 67:526–534. https://doi.org/10.1016/j.jhep.2017.04.024

12. Bakr S, Gevaert O, Patel B et al (2020) Interreader variability in semantic annotation of microvascular invasion in hepatocellular carcinoma on contrast-enhanced triphasic CT images. Radiol Imaging Cancer. https://doi.org/10.1148/rycan.2020190062. https://doi.org/10.1148/rycan.2020190062

13. Min JH, Lee MW, Park HS et al (2020) Interobserver variability and diagnostic performance of gadoxetic acid-enhanced MRI for predicting microvascular invasion in hepatocellular carcinoma. Radiology 297:573-581. https://doi.org/10.1148/radiol.2020201940

14. Chen J, Zhou J, Kuang S et al (2019) Liver Imaging Reporting and Data System Category 5: MRI Predictors of Microvascular Invasion and Recurrence After Hepatectomy for Hepatocellular Carcinoma. AJR Am J Roentgenol 213:821-830. https://doi.org/10.2214/AJR.19.21168

15. Segal E, Sirlin CB, Ooi C et al (2007) Decoding global gene expression programs in liver cancer by noninvasive imaging. Nat Biotechnol 25:675-80. https://doi.org/10.1038/nbt1306

16. Lambin P, Rios-Velazquez E, Leijenaar R et al (2012) Radiomics: extracting more information from medical images using advanced feature analysis. Eur J Cancer 48:441-6. https://doi.org/10.1016/j.ejca.2011.11.036

17. Miranda Magalhaes Santos JM, Clemente Oliveira B, Araujo-Filho JAB et al (2020) State-of-the-art in radiomics of hepatocellular carcinoma: a review of basic principles, applications, and limitations. Abdom Radiol (NY) 45:342-353. https://doi.org/10.1007/s00261-019-02299-3

18. Wakabayashi T, Ouhmich F, Gonzalez-Cabrera C et al (2019) Radiomics in hepatocellular carcinoma: a quantitative review. Hepatol Int 13:546-559. https://doi.org/10.1007/s12072-019-09973-0

19. Kim SH, Kamaya A, Willmann JK (2014) CT Perfusion of the liver: principles and applications in oncology. Radiology 272:322-44. https://doi.org/10.1148/radiol.14130091

20. Okada M, Kim T, Murakami T (2011) Hepatocellular nodules in liver cirrhosis: state of the art CT evaluation (perfusion CT/volume helical shuttle scan/dual-energy CT, etc.). Abdom Imaging 36:273-81. https://doi.org/10.1007/s00261-011-9684-2

21. Sahani DV, Holalkere NS, Mueller PR, Zhu AX (2007) Advanced hepatocellular carcinoma : CT perfusion of liver and tumor tissue--initial experience. Radiology 243:736-43. https://doi.org/10.1148/radiol.2433052020

22. Agrawal MD, Pinho DF, Kulkarni NM, Hahn PF, Guimaraes AR, Sahani DV. Oncologic Applications of Dual-Energy CT in the Abdomen. Radiographics. 2014;34:589-612. https://doi.org/10.1148/rg.343154041

23. Dai X, Schlemmer HP, Schmidt B et al (2013) Quantitative therapy response assessment by volumetric iodine-uptake measurement: initial experience in patients with advanced hepatocellular carcinoma treated with sorafenib. Eur J Radiol 82:327-34. https://doi.org/10.1016/j.ejrad.2012.11.013

24. Thaiss WM, Haberland U, Kaufmann S et al (2016) Iodine concentration as a perfusion surrogate marker in oncology: Further elucidation of the underlying mechanisms using volume perfusion CT with 80 kVp. Eur Radiol 26:2929-36. https://doi.org/10.1007/s00330-015-4154-9

25. Gordic S, Puippe GD, Krauss B et al (2016) Correlation between dual-energy and perfusion CT in patients with hepatocellular carcinoma. Radiology. 280:78-87. https://doi.org/10.1148/radiol.2015151560

26. Mulé S, Pigneur F, Quelever R et al (2018) Can dual-energy CT replace perfusion CT for the functional evaluation of advanced hepatocellular carcinoma? Eur Radiol 28:1977-1985. https://doi.org/10.1007/s00330-017-5151-y

27. Peduzzi P, Concato J, Kemper E, Holford TR, Feinstein AR (1996) A simulation study of the number of events per variable in logistic regression analysis. J Clin Epidemiol. 49:1373-9. https://doi.org/10.1016/s0895-4356(96)00236-3

28. Liu PH, Hsu CY, Hsia CY et al (2016) Prognosis of hepatocellular carcinoma: Assessment of eleven staging systems. J Hepatol. 64:601-8. https://doi.org/10.1016/j.jhep.2015.10.029

29. Lê S, Josse J, Husson F (2008). FactoMineR: An R Package for Multivariate Analysis. Journal of Statistical Software 25: 1–18. https://doi.org/10.18637/jss.v025.i01

30. Kolde R (2019) Pheatmap: Pretty Heatmaps. Implementation of heatmaps that offers more control over dimensions and appearance. https://CRAN.R-project.org/package=pheatmap

31. R Core Team (2022) R: A language and environment for statistical computing. R Foundation for Statistical Computing, Vienna, Austria. https://www.R-project.org

32. Ippolito D, Querques G, Okolicsanyi S, Franzesi CT, Strazzabosco M, Sironi S (2017) Diagnostic value of dynamic contrast-enhanced CT with perfusion imaging in the quantitative assessment of tumor response to sorafenib in patients with advanced hepatocellular carcinoma: A feasibility study. Eur J Radiol 90:34-41. https://doi.org/10.1016/j.ejrad.2017.02.027

33. Banerjee S, Wang DS, Kim HJ et al (2015) A computed tomography radiogenomic biomarker predicts microvascular invasion and clinical outcomes in hepatocellular carcinoma. Hepatology 62:792-800. https://doi.org/10.1002/hep.27877

34. Xu X, Zhang HL, Liu QP et al (2019) Radiomic analysis of contrast-enhanced CT predicts microvascular invasion and outcome in hepatocellular carcinoma. J Hepatol 70:1133-1144. https://doi.org/10.1016/j.jhep.2019.02.023

35. Ma X, Wei J, Gu D et al (2019) Preoperative radiomics nomogram for microvascular invasion prediction in hepatocellular carcinoma using contrast-enhanced CT. Eur Radiol 29:3595-3605. https://doi.org/10.1007/s00330-018-5985-y

36. Kim TM, Lee JM, Yoon JH et al (2020) Prediction of microvascular invasion of hepatocellular carcinoma: value of volumetric iodine quantification using preoperative dual-energy computed tomography. Cancer Imaging 2020;20(1):60. https://doi.org/10.1186/s40644-020-00338-7

37. Ji GW, Zhu FP, Xu Q et al (2020) Radiomic features at contrast-enhanced CT predict recurrence in early stage hepatocellular Carcinoma: A multi-institutional study. Radiology 294:568-579. https://doi.org/10.1148/radiol.2020191470

38. Taouli B, Hoshida Y, Kakite S et al (2017) Imaging-based surrogate markers of transcriptome subclasses and signatures in hepatocellular carcinoma: preliminary results. Eur Radiol 27:4472–4481. https://doi.org/10.1007/s00330-017-4844-6

39. García-Figueiras R, Goh VJ, Padhani AR et al (2013) CT perfusion in oncologic imaging: a useful tool? AJR Am J Roentgenol 200:8-19. https://doi.org/10.2214/AJR.11.8476

40. Zhu AX, Holalkere NS, Muzikansky A, Horgan K, Sahani DV (2008) Early antiangiogenic activity of bevacizumab evaluated by computed tomography perfusion scan in patients with advanced hepatocellular carcinoma. Oncologist 13:120-5. https://doi.org/10.1634/theoncologist.2007-0174

41. Van Beers BE, Leconte I, Materne R, Smith AM, Jamart J, Horsmans Y (2001) Hepatic perfusion parameters in chronic liver disease: dynamic CT measurements correlated with

disease severity. AJR Am J Roentgenol 176:667-73. https://doi.org/10.2214/ajr.176.3.1760667

42. Ronot M, Asselah T, Paradis V et al (2010) Liver fibrosis in chronic hepatitis C virus infection: differentiating minimal from intermediate fibrosis with perfusion CT. Radiology 256:135-42. https://doi.org/10.1148/radiol.10091295

43. Goh V, Halligan S, Bartram CI (2007) Quantitative tumor perfusion assessment with multidetector CT: are measurements from two commercial software packages interchangeable? Radiology 242: 777-82. https://doi.org/10.1148/radiol.2423060279

44. Bretas EAS, Torres US, Torres LR et al (2017) Is liver perfusion CT reproducible? A study on intra- and interobserver agreement of normal hepatic haemodynamic parameters obtained with two different software packages. Br J Radiol. 90(1078):20170214. https://doi.org/10.1259/bjr.20170214